A Novel Low Current Ripple Magnetically Coupled Interleaved DC-DC Buck-Boost Converter with High Efficiency and Continuous Transfer-Function for Fuel-Cell Applications

V.Samavatian, F.Mardani, M.Nourmohammadpour

Abstract— Efficiency, steady state analysis along with dynamic operation discussion of DC-DC converters are undoubtedly important issues in proficiency of renewable energy exploitation. This paper demonstrates the feasibility of using a DC-DC magnetically coupled interleaved DC-DC buck-boost converter for fuel-cell applications. While a step-up/step-down voltage transfer ratio has been achieved, the proposed converter exhibits non-pulsating I/O currents using interleave technique making it very suitable for renewable applications. Besides thoroughly elaboration of the steady state analysis, dynamic analysis including the converter control-to-output transfer function, which is continuous between two operation modes using I/O magnetic coupling, and a small signal ac equivalent circuit model based on state space averaging (SSA) method is also presented to help the designing of closed loop controllers for this proposed converter. Furthermore the experimental results are presented to verify the theoretical expected merits of the converter including high efficiency, non-pulsating I/O currents and continuous control-to-output transfer function. These Experimental results show impressive benefits of the proposed converter.

Index Terms— low-ripple I/O currents, magnetically coupled, high efficiency, continuous control-to-output transfer function, fuel cell.

1 INTRODUCTION

With ever-increasing use of renewable energy, crucial role of power electronic converters and their controlling methods have become fully evident in recent years. Studying and designing these converters is one of the most pressing concerns facing all electrical engineers. One of these converters extensively used in renewable energy resources such as battery charging, fuel cell systems, power factor correction (PFC), hybrid electric vehicles, communication power supply, maximum power point tracking (MPPT) of photovoltaic system (PVs) and for other renewable sources' maximum energy extraction, is DC-DC converters. Generally DC-DC converters divided into three main parts: buck, boost and buck-boost. Buck-boost converter has been employed since output voltage is within unregulated input voltage [1-9].

Despite conventional single-active-switch Buck-boost converter topologies including SEPIC, CUK, conventional inverting buck-boost and Flyback, non-inverting boost-buck converter made by cascaded connection of a boost converter to the buck converter is also achievable. It is indicated that this converter could be a reasonable choice in renewable energy power extractions due to its high efficiency and low component stresses in comparison with conventional single-active-switch buck-boost converters [2,3]. Beside above-mentioned step-up/step-down DC-DC converter topologies, a single inductor buck-boost converter which has high performance in the low voltage applications is thoroughly discussed in [5-7]. Regarding its topology, this converter is not suitable for high voltage/power applications. Another topology is KY buck–boost converter removing barrier of right half plane (RHP) zeros at the expense of increasing the number of switches resulting in increasing the cost of the device [10,11]. Most of the DC-DC converters mentioned earlier have the detriment of pulsating input/output (I/O) currents resulting in high noise level and complicated controlling system [3,4].In many applications low-ripple I/O current is absolutely essential especially in hybrid electric vehicles, power factor correction, fuel cell, etc [12-14]. The two-switch tri-state buck-boost has been used in order to mitigate this problem [15] and regarding capability of using large inductance in pseudo-continuous conduction mode (PCCM) [16], [17], lower-ripple I/O currents can be readily achieved. However efficiency of this converter declines owing to the increase in the number of active switches. Using interleaved technique including the benefits such as harmonic cancellation, better efficiency, component stresses reduction, better thermal performance, and high power density is another solution that can be easily acquired [12, 14, 18-21]. Although the concept of this technique is not newly introduced, wide areas of applications are covered by this technique [22]. In [12], the 16-phase interleaved bidirectional boost topology for hybrid energy storage system (HESS) has solved I/O currents high ripple but this topology has just discussed the boost converter and it is

- *Vahid Samavatian received the M.S. degree from K.N.Toosi University of Technology, Tehran, Iran, and He is currently working toward the Ph.D. degree in the University of Tehran, Tehran, Iran*
  E-mail: vahidsamavatian@ee.kntu.ac.ir
- *Fatemeh Mardani Received the M.S. degree in Electrical Engineering, Electrical Machine & Power Electronics, from the K.N.Toosi University of Technology, Tehran, Iran.*
  E-mail: fateme.mardani68@gmail.com
- *Mohammad Nourmohmmadpour received the M.S. degree in Electrical Engineering, Electrical Machine & Power Electronics, from K. N.Toosi University of Technology, Tehran, Iran.*
  E-mail: m.nourmohammadpour@ee.kntu.ac.ir

not generalized in buck-boost converters. In [14], H.K. Liao et al, have proposed an interleaved non-inverting buck-boost converter with a low-output current ripple, but in this topology mitigating the input voltage variation in wide range is not achieved. Although the double-switch buck–boost converter proposed in [19] can reduce the current ripple, component stresses have been remained high through this topology resulting in low efficiency. Another solution reported here is to utilize a non-inverting interleaved buck-boost converter. This proposed topology is used in order to improve I/O currents ripple, converter's efficiency and reduce component stresses. In addition, because input and output inductances are magnetically related to each other, the small signal control-to-output transfer function dissociation at boundary mode of proposed converter which is a major problem in double-active-switch buck-boost converters is readily solved. This proposed converter can be easily used as a modular converter suitable for high transferring power density. The purpose of this paper is to analyze cascaded combination of an interleaved boost with an interleaved buck converter magnetically coupled and shown in Fig. 1. Organization of this paper is as follows. Section II discusses principle of operation and steady state analysis based on the depicted key waveforms of proposed converter. Dynamic Analysis and small signal modeling are thoroughly studied in section III. In section IV, circuit design and its implementation have been presented. Section V focuses on the experimental results in both operation modes and under different conditions. Finally, the last section presents conclusion of this study.

2 PRINCIPLE OF OPERATION AND STEADY STATE ANALYSIS

Proposed converter is shown in Fig. 1. This converter can operate either in boost mode or buck mode as shown in Fig. 2(a) and Fig. 2(b) respectively. As shown in Fig. 2 the boost mode would be achieved provided that the switches 3 and 4 are permanently turning on and switches 1 and 2 working in PWM manner, while in the buck mode switches 1 and 2 are permanently turning off and switches 3 and 4 working in PWM manner.

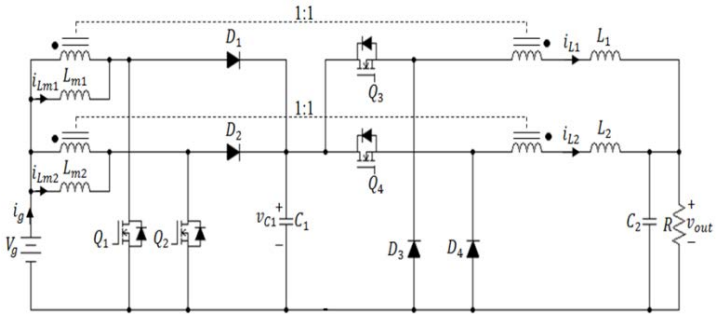

Fig .1. Schematic circuit diagram of proposed converter

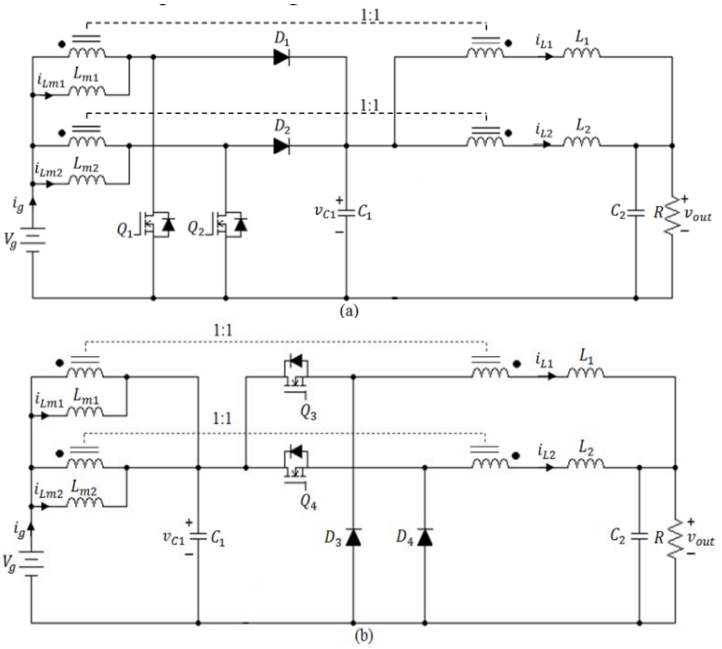

Fig. 2. Operating modes of proposed converter: (a) boost mode; (b) buck mode.

The steady state operation waveforms of this converter for both modes of boost and buck are illustrated in Fig. 3(a) and (b) respectively. The last curves in these two figures, S_1 to S_4, are allocated to logic activation signals of Q_1 to Q_4 The PWM activation signals of Q_1 and Q_2 are similar to each other with a phase shift of $T_S / 2$ for catering the interleaved pattern. In the boost mode the duty ratios of the boost stage (Q_1 and Q_2 activation signals) are considered to be $d_{12}(t)$. The same is true for Q_3 and Q_4 activation signals with the duty ratio $d_{34}(t)$ in the buck mode. The duty ratio of switches is adjusted so that the output voltage is regulated around a desired value (here 36 V) in both operational modes. In addition, through increasing the number of interleaved phase in boost and buck stages, the proposed converter can be easily used as a modular converter being suitable for transferring high power density in applications such as HESS and other individual storage systems. For extracting the principles of operation and determining the modeling equations for both modes of operation, the switching pattern of Fig. 4 is employed. By resorting this switching pattern, all possible converter switching states will be considered. Regarding this figure, each period consists of 6 time intervals and 6 corresponding circuit diagrams depicted in Fig. 5. Time interval numbering and portioning are mentioned in Table. 1. Since the intervals 2 and 5 have the same time portions and switching states, (see Fig. 4 and Fig. 5), the converter can be analyzed only in 5 states as follows:

Interval 1:[$t_0 - t_1$], Fig. 5(a), In this time interval Q_1, Q_3 and Q_4 are in conducting mode making the magnetizing inductor 1 to

start saving energy and simultaneously magnetizing inductor 2 to transfer its stored energy to the output load and inductors through D_2. With regard to Fig. 5(a), the differential equations describing the voltage across the capacitors and current passing through the inductors in the first time interval can be evaluated as follows:

$$\begin{cases} v_{Lm1}(t) = L_{m1}\dfrac{di_{Lm1}}{dt} = v_g(t) \\ v_{Lm2}(t) = L_{m2}\dfrac{di_{Lm2}}{dt} = v_g(t) - v_{C1}(t) \\ v_{L1}(t) = L_1\dfrac{di_{L1}}{dt} = v_g(t) + v_{C1}(t) - v_{out}(t) \\ v_{L2}(t) = L_2\dfrac{di_{L2}}{dt} = v_g(t) - v_{out}(t) \\ i_{c1}(t) = C_1\dfrac{dv_{C1}}{dt} = i_{Lm2}(t) - i_{L1}(t) \\ i_{c2}(t) = C_2\dfrac{dv_{C2}}{dt} = i_{L1}(t) + i_{L2}(t) - \dfrac{v_{out}(t)}{R} \end{cases} \quad (1)$$

Interval 2 and 5: $[t_1 - t_2$ and $t_4 - t_5]$, Fig. 5(b), in this time interval Q_3 and Q_4 are in conducting mode while Q_1 and Q_2 are turning off. Accordingly the energy stored in magnetizing inductors 1and 2 starts transferring to inductors 1 and 2 through D_1 and D_2. Similarly, a set of differential equations can be found for describing the voltage across the capacitors and current passing through the inductors for other time intervals, but for briefness these equations have not been written.

Interval 3: $[t_2 - t_3]$, Fig. 5(c), in this time interval Q_3 is in conducting mode while Q_1, Q_2 and Q_4 are off. Energy transfer in this interval is thoroughly similar to the previous interval except that the energy stored in both input magnetizing inductors is only transferred to the inductor 1.

Interval 4: $[t_3 - t_4]$, Fig. 5(d), in this time interval Q_2, Q_3 and Q_4 are conducting while Q_1 is turning off. Energy transfer in this interval is also similar to that of interval 1 except that the functions of magnetizing inductors 1 and 2 replace each other.

Interval 6: $[t_5 - t_6]$, Fig. 5(e), in this time interval Q_4 is in conducting mode while Q_1, Q_2 and Q_3 are off. Accordingly the energy saved in magnetizing inductor 1 and 2 is transferred to the output capacitor and inductor 2.

Table.1. required expressions for evaluating parameters' values

Interval number	Time interval	Time portion
1	$t_0 - t_1$	$d_{12}(t)T_s$
2	$t_1 - t_2$	$(d_{34}(t) - d_{12}(t) - 0.5)T_s$
3	$t_2 - t_3$	$(1 - d_{34}(t))T_s$
4	$t_3 - t_4$	$d_{12}(t)T_s$
5	$t_4 - t_5$	$(d_{34}(t) - d_{12}(t) - 0.5)T_s$
6	$t_5 - t_6$	$(1 - d_{34}(t))T_s$

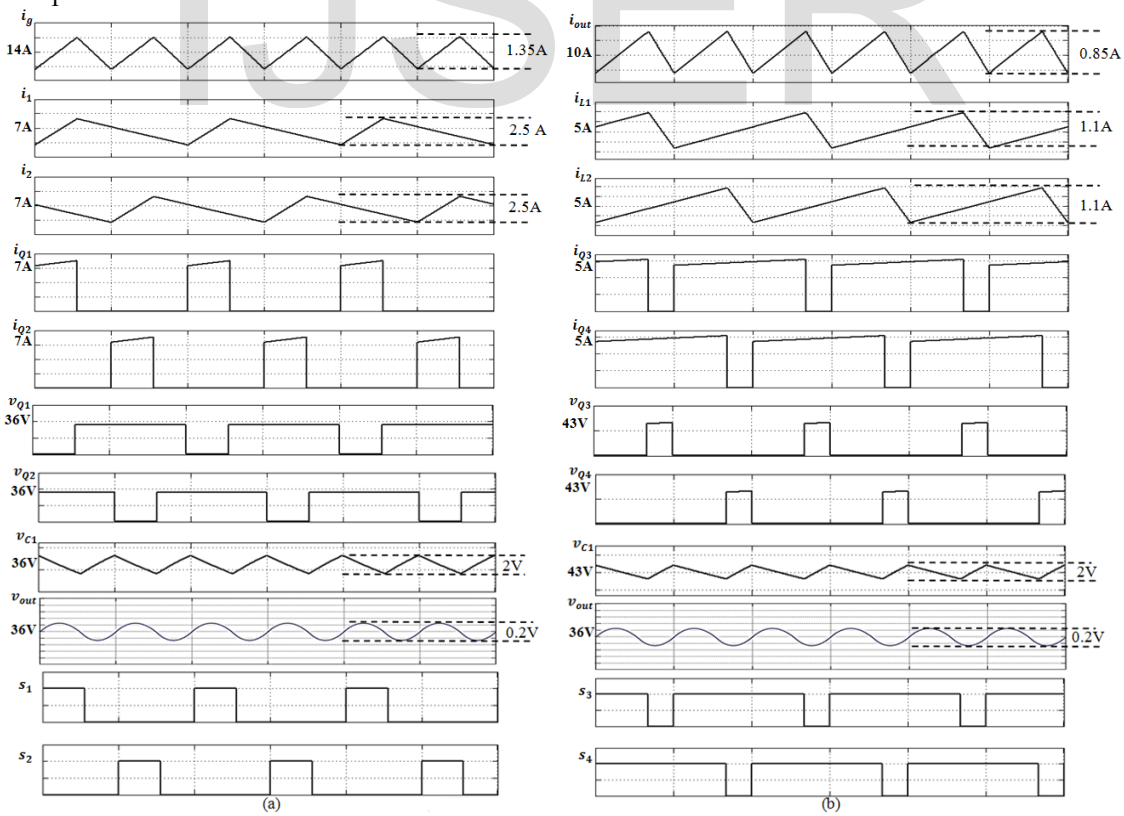

Fig. 3. Key waveforms of converter shown in Fig. 1 for $V_{out} = 36\ V$, (a) currents and voltages in boost mode with $V_g = 26\ V$ (D_{34}=1), (b) currents and voltages in buck mode with $V_g = 43\ V$ ($D_{12} = 0$)

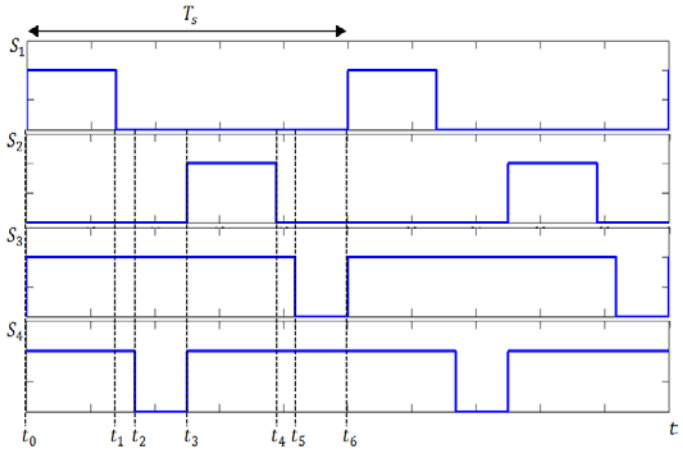

Fig. 4. Switching pattern of converters' switches

To the authors' knowledge two reported methods are employed for obtaining the differential equations portraying the behavior of all interleaved converters, namely, state space averaging (SSA) methods [16] and signal flow graph (SFG) [37]. In this work state space averaging method is selected owing to its simplicity.

With the assumptions of continuous conduction mode (CCM) working and a switching frequency much higher than the converter natural frequencies, SSA method [16] can be applied to determine the converter model regarding the small-ripple approximation and the principles of inductor volt-second balance and capacitor charge balance.

Using the differential equations of all time intervals and exerting averaging technique [16] on evaluated equations over one switching period, it yields:

$$\begin{cases} L_{m1}\langle\frac{di_{Lm1}(t)}{dt}\rangle_{T_s} = V_g(t) - V_{C1}(t)\big(1-d_{12}(t)\big) \\ L_{m2}\langle\frac{di_{Lm2}(t)}{dt}\rangle_{T_s} = V_g(t) - V_{C1}(t)\big(1-d_{12}(t)\big) \\ L_1\langle\frac{di_{L1}(t)}{dt}\rangle_{T_s} = V_g(t) - V_{out}(t) + V_{C1}(t)(d_{34}(t)+d_{12}(t)-1) \\ L_2\langle\frac{di_{L2}(t)}{dt}\rangle_{T_s} = V_g(t) - V_{out}(t) + V_{C1}(t)(d_{34}(t)+d_{12}(t)-1) \\ C_1\langle\frac{dV_{C1}(t)}{dt}\rangle_{T_s} = \big(i_{Lm1}(t)+i_{Lm2}(t)\big)\big(1-d_{12}(t)\big) \\ \qquad\qquad +\big(i_{L1}(t)+i_{L2}(t)\big)\big(1-d_{12}(t)-d_{34}(t)\big) \\ C_2\langle\frac{dV_{out}(t)}{dt}\rangle_{T_s} = (i_{L1}(t)+i_{L2}(t)) - \frac{V_{out}}{R} \end{cases} \quad (2)$$

Where d_{12} *and* d_{34} are the duty ratios of the switches $[Q_1, Q_2]$ and $[Q_3, Q_4]$ respectively. For attaining the current passing through the converter inductors and the voltage across the converter capacitors in steady states condition, one may use the steady state operating value of duty ratios, D_{12} *and* D_{34}, and input voltage, V_g, and exert the principles of inductor volt-second and capacitor charge balance to obtain another set of expressions describing the steady state operation as follows:

$$\begin{cases} I_g = I_{Lm1} + I_{Lm2} + I_{L1} + I_{L2} = \frac{D_{34}}{1-D_{12}}\frac{V_{out}}{R} \\ I_{out} = I_{L1} + I_{L2} = \frac{V_{out}}{R} \\ V_{C1} = \frac{V_g}{1-D_{12}} = \frac{V_{out}}{D_{34}} \\ V_{out} = D_{34}V_{C1} = \frac{D_{34}}{1-D_{12}}V_g \end{cases} \quad (3)$$

The last expression of equation 3 is the voltage transfer ratio of converter M (D_1, D_2) as follows:

$$\mathrm{M}\,(D_{12}\,,\,D_{34}) = \frac{V_{out}}{V_g} = \frac{D_{34}}{1-D_{12}} \quad (4)$$

The converter operation in both boost and buck modes is defined by the following conditions.

$$\begin{aligned} &\text{Boost mode:} \quad \{D_{34} = 1 \text{ and } 0 < D_{12} < 1\} \\ &\text{Buck mode:} \quad \{D_{12} = 0 \text{ and } 0 < D_{34} < 1\} \end{aligned} \quad (5)$$

For a smooth transition between the two modes of operation, voltage transfer ratio M (D_{12}, D_{34}) should be written in terms of only one control variable [17], [19]. To establish a meaningful relation between D_{12} *and* D_{34}, the variable u is defined:

$$u = D_{12} + D_{34} \quad (6)$$

$$\begin{aligned} &\text{Therefore, for Boost mode:} \quad 1 < u < 2 \\ &\text{And for Buck mode:} \quad 0 < u < 1 \end{aligned} \quad (7)$$

Regarding this new variable, the modified voltage conversion ratio can be written as follows.

$$M(u) = \frac{\min(1,u)}{1-\max(0,u-1)} \quad (8)$$

Employing equation (8) as voltage conversion ratio, a smooth transition between the two modes of operation can be easily guaranteed. The voltage conversion ratio in term of u is illustrated in Fig. 6.

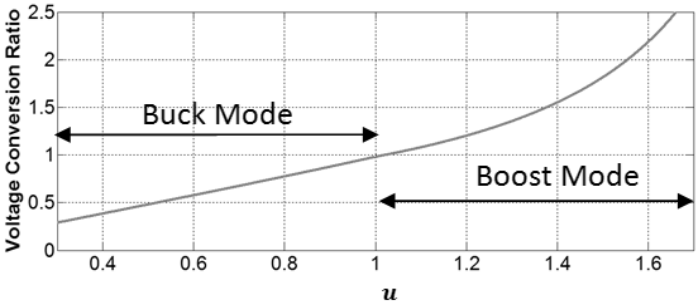

Fig. 6.Voltage Conversion ratio of the proposed buck-boost converter

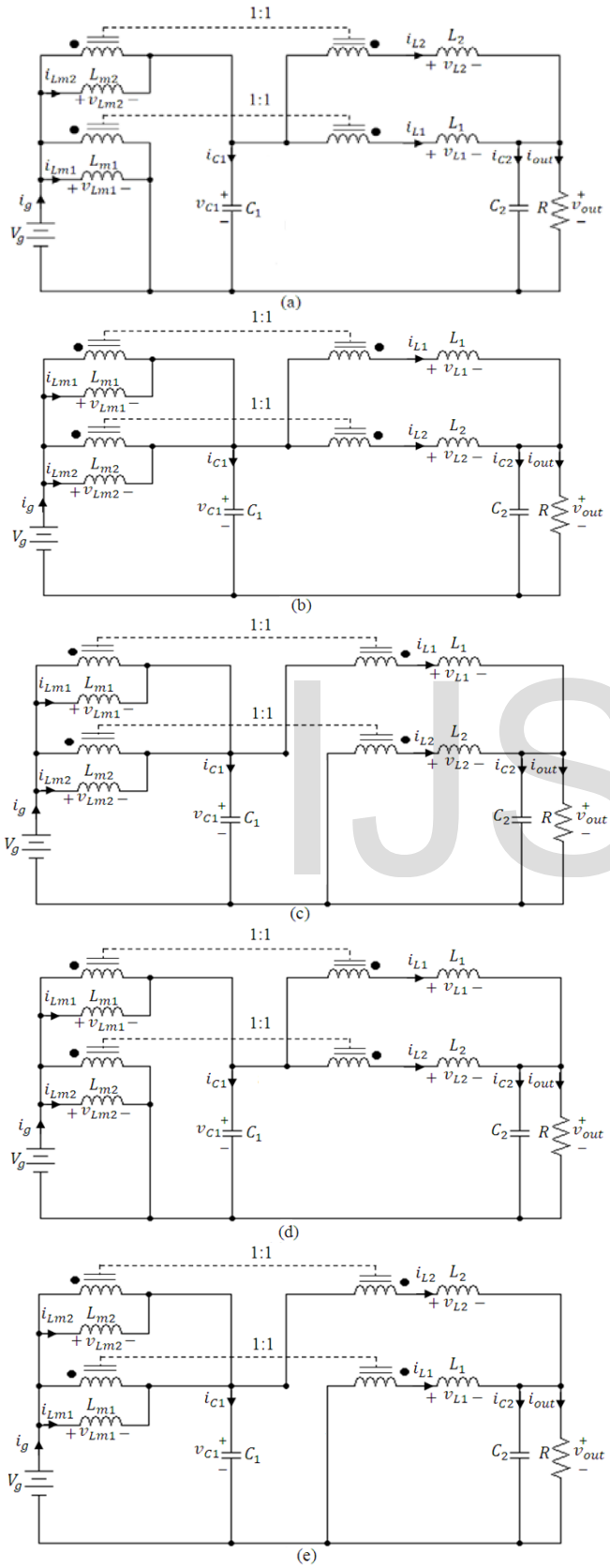

Fig. 5.Operating states. (a) circuit diagram in interval 1,(b) circuit diagram in interval 2,5,(c) circuit diagram in interval 3, (d) circuit diagram in interval 4, (e) circuit diagram in interval 6.

3 DYNAMIC ANALYSIS OF THE PROPOSED CONVERTER

To obtain the small signal model around the specific operating point, the input voltage, $V_g(t)$, and duty ratios, $d_{12}(t)$ and $d_{34}(t)$, are assumed as a constant value of V_g, D_1 and D_2 plus some small ac variations, $\hat{V}_g(t)$, $\hat{d}_{12}(t)$ and $\hat{d}_{34}(t)$ respectively.

$$\begin{cases} V_g(t) = V_g + \hat{V}_g(t) \\ d_{12}(t) = D_{12} + \hat{d}_{12}(t) \\ d_{34}(t) = D_{34} + \hat{d}_{34}(t) \end{cases} \tag{9}$$

By applying above inputs, the inductor currents and capacitor voltages can be stated with their steady state plus their small ac variations determined by

$$\begin{cases} i_{Lm1}(t) = I_{Lm1} + \hat{\imath}_{Lm1}(t) \\ i_{Lm2}(t) = I_{Lm2} + \hat{\imath}_{Lm2}(t) \\ i_{L1}(t) = I_{L1} + \hat{\imath}_{L1}(t) \\ i_{L2}(t) = I_{L2} + \hat{\imath}_{L2}(t) \\ v_{C1}(t) = V_{C1} + \hat{v}_{C1}(t) \\ v_{C2}(t) = V_{C2} + \hat{v}_{C2}(t) \end{cases} \tag{10}$$

Now the set of differential equations (2) can be linearized around their operating point values providing that the ac variations are much smaller than the steady state values at operating point. Employing this analysis along with separating just first-order terms of resulted equations, following set of equations of inductor voltages and capacitor currents can be readily acquired.

$$\begin{cases} \hat{v}_{Lm1}(t) = \hat{v}_{Lm2}(t) = \hat{v}_g(t) - \hat{v}_{C1}(t)(1 - D_{12}) + V_{C1}\hat{d}_{12}(t) \\ \hat{v}_{L1}(t) = \hat{v}_{L2}(t) = \hat{v}_g(t) - \hat{v}_{out}(t) + \hat{v}_{C1}(t)(D_{34} + D_{12} - 1) \\ \qquad\qquad + V_{C1}(\hat{d}_{34}(t) + \hat{d}_{12}(t)) \\ \hat{\imath}_{C1}(t) = \hat{\imath}_g(t)(1 - D_{12}) - \big(\hat{\imath}_{L1}(t) + \hat{\imath}_{L2}(t)\big)D_{34} - I_g\hat{d}_{12}(t) \\ \qquad\qquad - \dfrac{V_{out}}{R}\hat{d}_{34}(t) \\ \hat{\imath}_{C2}(t) = \hat{\imath}_{L1}(t) + \hat{\imath}_{L2}(t) - \dfrac{\hat{v}_{out}(t)}{R} \end{cases} \tag{11}$$

Regarding (11), one can consider an input and output inductors whose values are equal to the value of L_{m1} and L_{m2} and L_1 and L_2 connecting in parallel respectively. Let us define:

$$\begin{cases} L_{m12} = L_{m1} \| L_{m2} \\ L_{12} = L_1 \| L_2 \end{cases} \tag{12}$$

$$\begin{cases} \hat{\imath}_{Lm12}(t) = \hat{\imath}_{Lm1}(t) + \hat{\imath}_{Lm2}(t) \\ \hat{\imath}_{L12}(t) = \hat{\imath}_{L1}(t) + \hat{\imath}_{L2}(t) \end{cases} \tag{13}$$

Now with using (11), the small signal ac equivalent circuit model can be obtained [3]. Fig. 7 illustrates small signal ac equivalent circuit model of proposed converter.

By above definition and defining state space vector $\hat{x}$ as (14) and state space equation as (15) and by linearizing (2) around (3) and separating just first-order terms of resulted equations, it yields

$$\hat{x} = [\,\hat{\imath}_{Lm12}\hat{\imath}_{L12}\hat{v}_{C1}\hat{v}_{out}]^T \tag{14}$$

$$\frac{d\hat{x}}{dt} = A\hat{x} + B\hat{U} \tag{15}$$

$$\hat{U} = [\,\hat{V}_g\hat{d}_{12}\hat{d}_{34}]^T \tag{16}$$

Where A is state matrix and B is input vector corresponding to $\hat{V}_g$, $\hat{d}_{12}(t)$ and $\hat{d}_{34}(t)$.

$$A = \begin{bmatrix} 0 & 0 & \frac{D_{12}-1}{L_{m12}} & 0 \\ 0 & 0 & \frac{D_{12}+D_{34}-1}{L_{12}} & \frac{-1}{L_{12}} \\ \frac{1-D_{12}}{C_1} & \frac{1-D_{12}-D_{34}}{C_1} & 0 & 0 \\ 0 & \frac{1}{C_2} & 0 & \frac{-1}{RC_2} \end{bmatrix} \tag{17}$$

$$B = \begin{bmatrix} \frac{1}{L_{m12}} & \frac{V_{out}}{D_{34}L_{m12}} & 0 \\ \frac{1}{L_{12}} & \frac{V_{out}}{D_{34}L_{12}} & \frac{V_{out}}{D_{34}L_{12}} \\ 0 & \frac{-D_{34}}{1-D_{12}}\frac{V_{out}}{RC_1} & -\frac{V_{out}}{RC_1} \\ 0 & 0 & 0 \end{bmatrix} \tag{18}$$

Accordingly in the boundary mode, namely D_{12} and D_{34} are equal to 0 and 1 values respectively, the small signal control-to-output transfer functions with respect to $\hat{d}_{12}(t)$ and $\hat{d}_{34}(t)$ can be given by following expressions respectively.

$$\begin{cases} G_{vod12}(s) = \dfrac{\hat{v}_{out}(s)}{\hat{d}_{12}(s)} = \dfrac{\lambda(s)V_gR}{\lambda(s)(L_{12}RC_2s^2 + L_{12}s + R)} \\ G_{vod34}(s) = \dfrac{\hat{v}_{out}(s)}{\hat{d}_{34}(s)} = \dfrac{\lambda(s)V_gR}{\lambda(s)(L_{12}RC_2s^2 + L_{12}s + R)} \\ \lambda(s) = L_{m12}C_1s^2 + 1 \end{cases} \tag{19}$$

With regard to the above equations, continuous behavior is achieved between two operation modes using magnetic coupling. Employing the following parameter values (completely explained in the following section), $L_{m12} = 100\mu H$, $L_{12} = 100\mu H$, $C_1 = C_2 = 10\mu f$ and $R = 3.6\Omega$, the bode diagram of control-to-output transfer functions in boundary mode is depicted in Fig. 8 in terms of three different load conditions $R = 3.6\Omega$, $R = 7.2\Omega$ and $R = 18\Omega$. It is easily seen that in this mode phase margin (PM) is not large enough to guarantee the stability of closed loop system. This problem can be easily solved by designing a suitable classic controller. Furthermore by increasing load to its nominal value, it can also be observed that in this mode PM would be boomed.

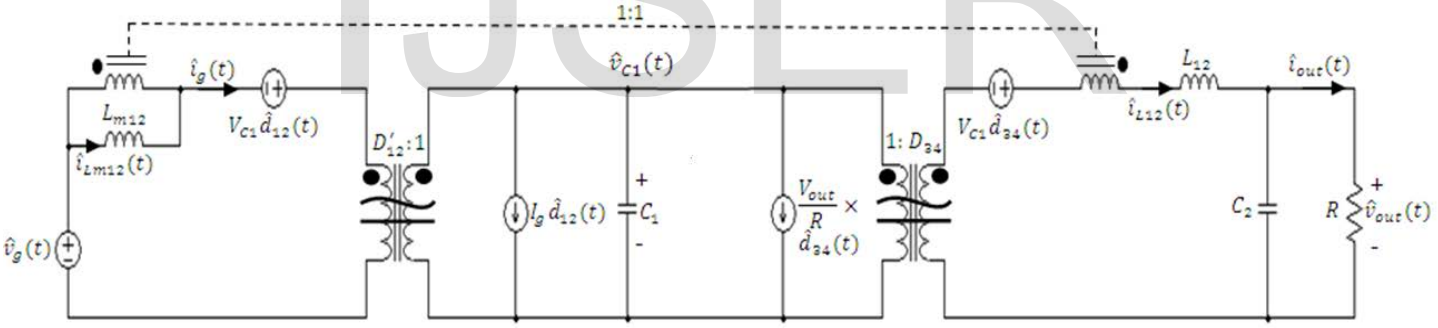

Fig. 7. Small signal ac equivalent circuit model for converter

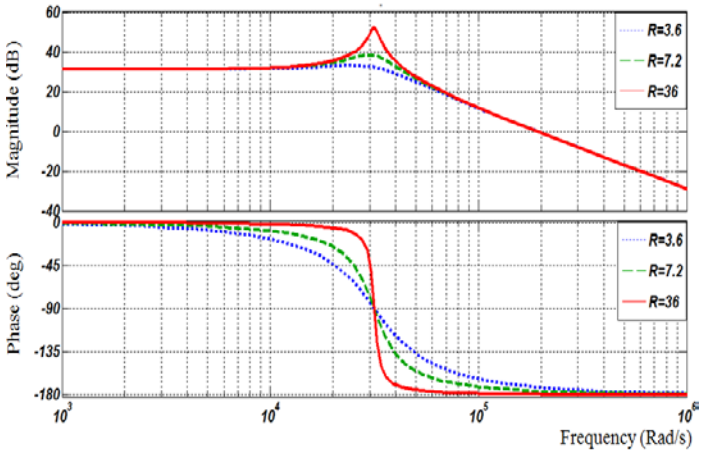

Fig. 8. Frequency response of the small-signal control-to-output transfer function in the boundary mode.

4 CIRCUIT DESIGN

The proposed converter is designed as fuel cell regulation device so that its input voltage range varies from 26V to 43V. The maximum output power is 360W. Regarding output voltage value, 36V, corresponding load resistance is 3.6 Ohm By above data it can be easily observed that duty ratios are limited to $0 < D_{12} < 0.2777$ and $0.833 < D_{34} < 1$ in boost and buck operation modes respectively. The switching frequency is fixed around 25 KHz and as a consideration the inductors currents ripples are restricted to 1.5A while output capacitor and intermediate capacitor voltage ripples are respectively limited to 0.2 V and 2V. Expressions required for calculating values of capacitors and inductors in both operation modes can easily obtained from differential equations described in section II

and the final circuit design equations listed in Table. 2.

5 EXPERIMENTAL RESULTS

5.1 Converter Power Stage

Fig. 9 has shown the top view of power stage prototype. The components have been individually introduced on this figure. In this section, the behavior of proposed converter in the steady state condition with applying V_g equal to 26V in boost mode and 43V in buck mode under full load condition will be discussed. Furthermore, dynamic responses led by load and input voltage changes will be separately studied in two different operation modes. The design matches a fuel cell voltage regulation, with the brand of "FCgen 1020ACS" Ballard Power Systems, Inc. regarding design equations, the components list and their values are given in Table. 3.

5.2 Control Circuit

Employing Fig. 8 and classical rules of designing a linear compensation network in frequency domain [3] for increasing the stability margin in both operation modes, the following second-order compensator transfer function can be evaluated.

$$G_c(s) = \frac{1000(s+3241)(s+1414)}{s(s+696625)} \tag{20}$$

The circuit diagram of the above compensator and the pulse width modulation (PWM) are depicted in Fig. 10 where switching dispositions has been added for catering interleaves technique. One should notice that by considering this circuit diagram an effective analogue controller for the converter can be easily achieved using a few conventional simple components.

Table.3. Components for proposed converter

component	Boost Mode	Buck Mode	Selected
L_{m1or2}	192.5 µH	3.33 µH	200 µH
L_{1or2}	192.5 µH	156.24 µH	200 µH
C_1	20.13 µF	20.11 µF	20 µF
C_2	19.375 µF	19.375 µF	20 µF
Q_1, Q_2, Q_3, Q_4	-	-	IRF840b
D_1, D_2, D_3, D_4	-	-	MBR20100

Table. 2 Expressions required for calculating converter values in CCM

components	Boost mode	Buck mode	Desired value
L_{m1or2}	$\frac{V_g D_{12} T_s}{\Delta i_{Lm1or2_{Boost}{}^{p-p}}}$	$\frac{\Delta v_{C1Buck}{}^{p-p} T_s}{16\, \Delta i_{Lm1or2_{Buck}{}^{p-p}}}$	Max{Boost, Buck}
L_{1or2}	$\frac{V_g D_{12} T_s}{\Delta i_{L1or2_{Boost}{}^{p-p}}}$	$\frac{(V_g - V_{out}) D_{34} T_s}{\Delta i_{L1or2_{Buck}{}^{p-p}}}$	Max{Boost, Buck}
C_1	$\frac{\frac{V_{out}}{R}\frac{D_{12}}{(1-D_{12})}(1-2D_{12})\frac{T_s}{2}}{\Delta v_{C1_{Boost}{}^{p-p}}}$	$\frac{\frac{V_{out}}{R}(D_{34}-1)(2D_{34}-1)\frac{T_s}{2}}{\Delta v_{C1_{Buck}{}^{p-p}}}$	Max{Boost, Buck}
C_2	$\frac{1}{32}\frac{\Delta i_{L1or2_{Boost}{}^{p-p}}}{\Delta v_{C2_{Boost}{}^{p-p}}} T_s$	$\frac{1}{32}\frac{\Delta i_{L1or2_{Buck}{}^{p-p}}}{\Delta v_{C2_{Buck}{}^{p-p}}} T_s$	Max{Boost, Buck}

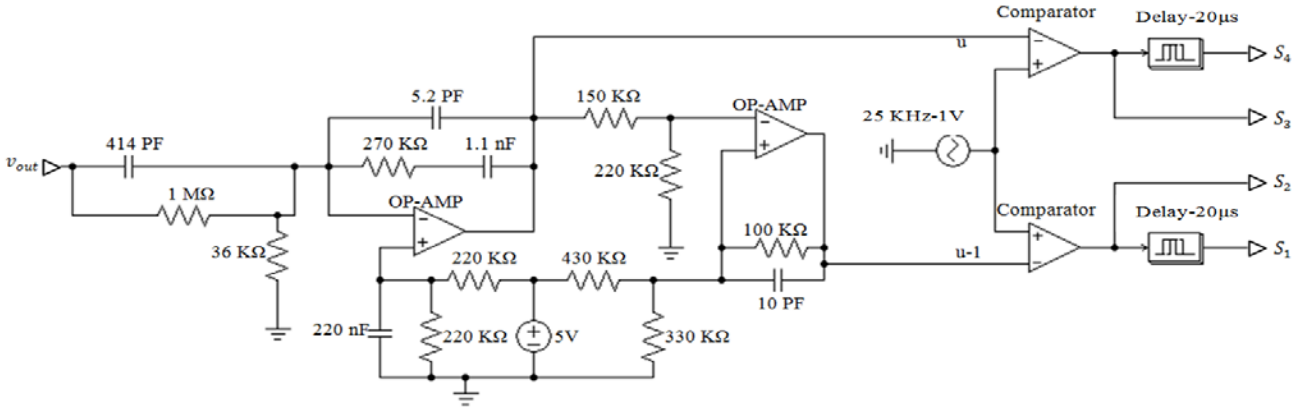

Fig. 10.Schematic of compensation network using analogue circuit

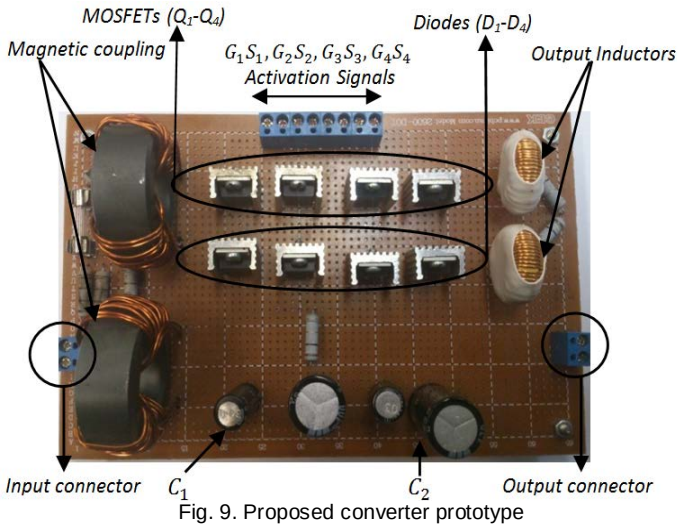

Fig. 9. Proposed converter prototype

The activation signals in boost mode are depicted in Fig. 11a where $D_{34}=1$ and D_{12} are operating in PWM mode and those are shown in Fig. 11b where $D_{12}=0$ and D_{34} are operating in PWM mode respectively. As it can be seen in Fig. 11 the activation signals either in boost mode or in buck mode have a delay of $T_S/2$. This delay guarantees the procedure of interleaving technique which is one of the most important aims of this proposed converter. Figs. 12a and 12b show the input, output and inductor currents in boost and buck operation modes respectively. As illustrated from these figures, the maximum ripple is limited to 1.5A for the inductor currents (%11.5) and to 1A (%10) for input and output currents respectively. The voltage ripples of intermediate capacitor and output capacitor in both operation modes are depicted in Figs. 13a and 13b. Maximum ripple of intermediate capacitor and output capacitor voltages are restricted to 2V, 0.2V (%0.5), respectively. Not only these properties satisfactorily meet the application requirements, but also when compared to the other recent studies [4], [11], [14], [16] with input current ripple percentages as large as %20, %23, %30 and %30 respectively, proves an enhanced steady state performance for this converter. The dynamic behaviors of this converter during applying a load change between half rated (180W) and full rated (360W) for both boost and buck operation modes are depicted in Fig. 14(a) and Fig. 14(b) respectively. Employing compensation network given in (20), one can find that only a voltage change of 1.8V (5%) in boost mode and about 2.5V (6.9%) in buck mode occurs once the load change is applied and the converter encounters no internal oscillation. The dynamic responses of proposed converter output voltage to large input voltage variation under full load condition are illustrated in Fig. 15. In boost mode, input voltage increases from 26V to 36V and then decreases to its initial value while in buck mode input voltage decreases from 43V to 36V and then increases to its initial value. This figure depicts that the maximum overshoot is strictly kept less than 1.1V (3%) in both operation modes.

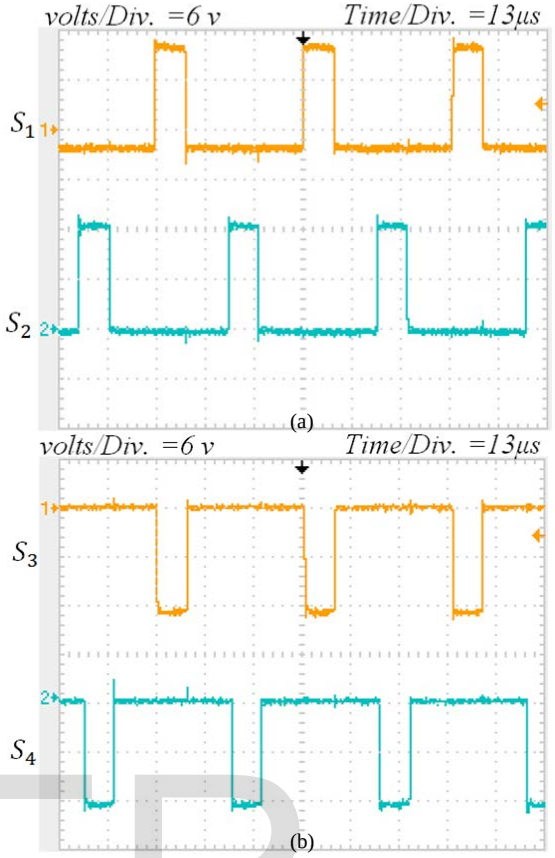

Fig. 11.Activation signals, (a) boost mode, (b) buck mode

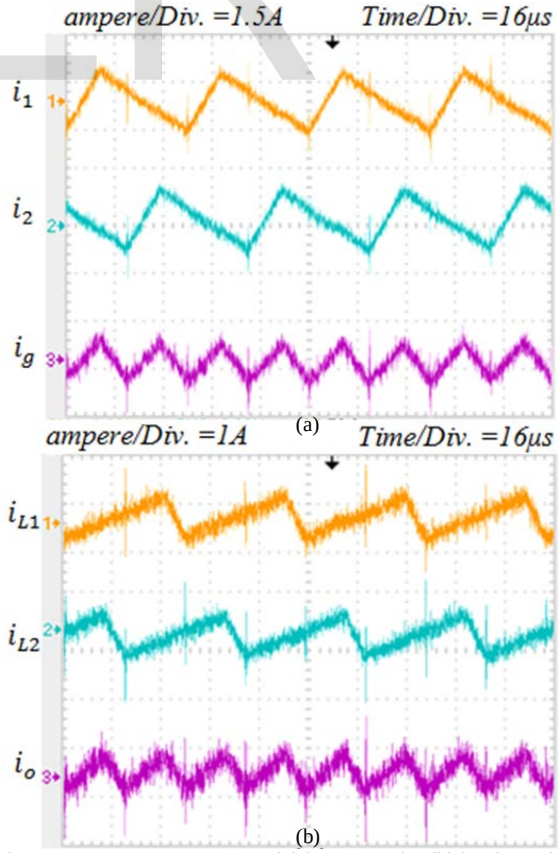

Fig. 12. Converters' currents, (a) boost mode, (b) buck mode

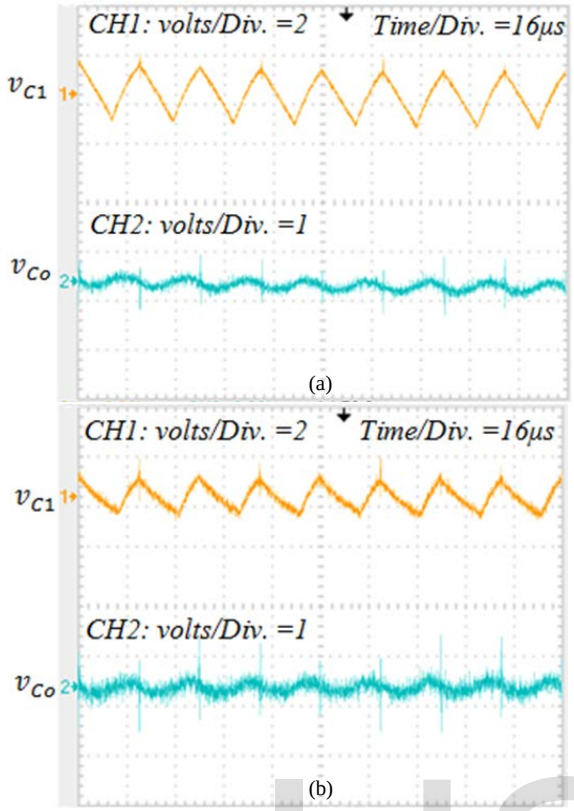

Fig. 13. Converters' voltages, (a) boost mode, (b) buck mode

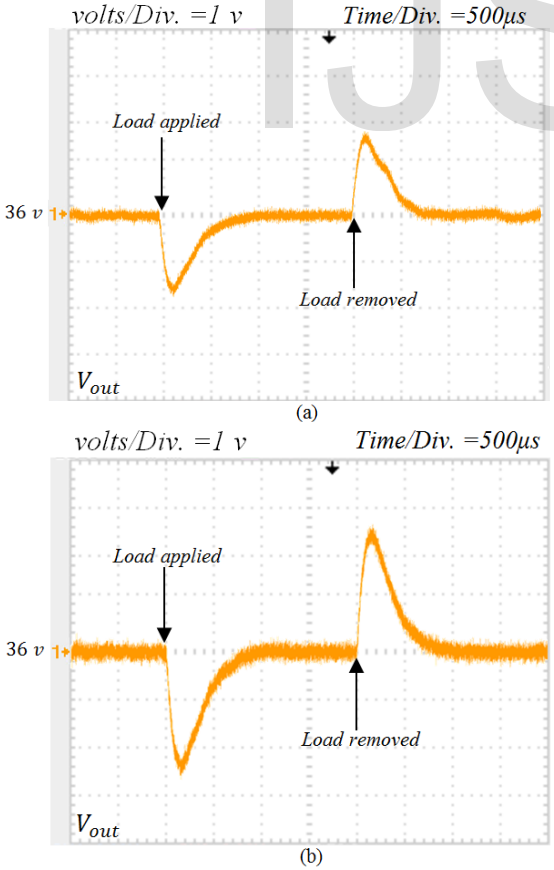

Fig. 14. Output voltage variations during applying and removing load from its half rated (180W) to its rated (360W). (a) Boost mode, (b) Buck mode.

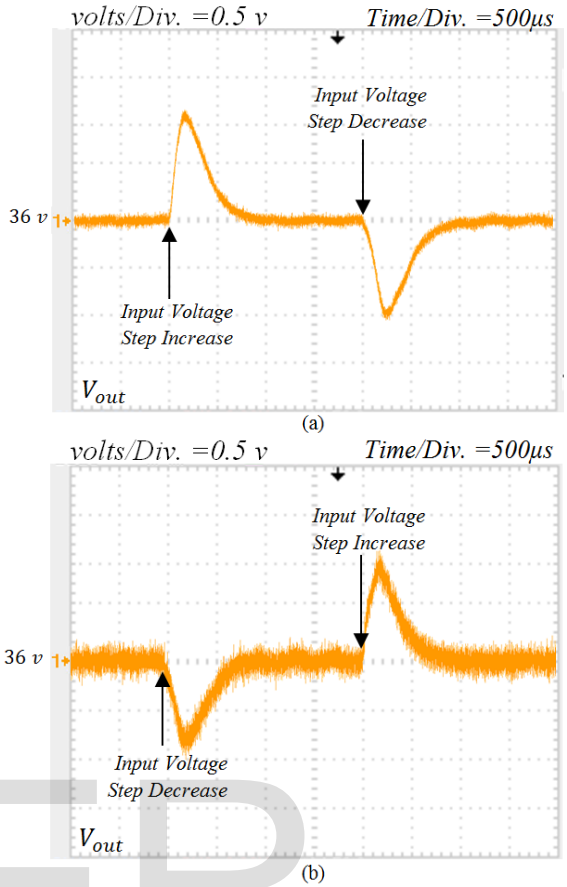

Fig. 15. Output voltage variations during input voltage step changes, (a) boost mode, (b) buck mode.

The energy conversion efficiency is a major issue of any conversion system. Efficiency traces as a function of the input voltage for different output current levels are shown in Fig. 16. Regarding this figure, Maximum efficiency as a function of the input voltage with different output current levels occurs in all current levels when input voltage is near to 36 V. Because in this case, buck and boost switches are permanently on and off respectively and there is only conduction power loss.

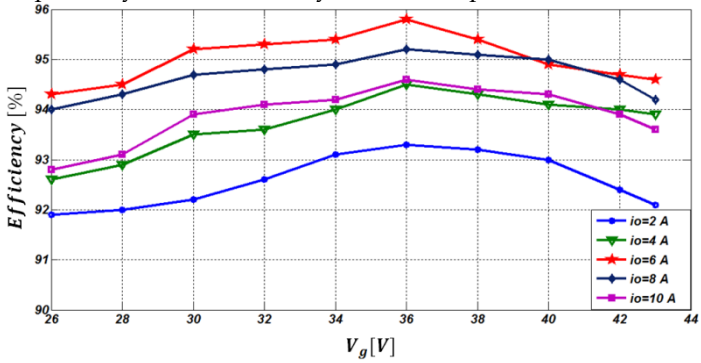

Fig. 16. Energy conversion efficiency for Vo= 36 V as function of the input voltage for different output current levels.

6 CONCLUSION

A non-inverting I/O magnetically coupled buck–boost DC–DC converter obtained through a cascade connection of an interleaved boost and an interleaved buck stage, is discussed.

Mathematical analyses, simulation and experimental results of a prototype converter validate the predicted low-ripple I/O currents due to interleaved technique employment. Efficiency studies show that the maximum efficiency can be achieved in the boundary mode where the boost stage switches are always OFF and the buck stage switches are continuously ON.In addition, converter small signal modeling is explored to help the control design. Dynamic studies show that the maximum overshoot is limited to 7% in the load changes while it is about 3% in the input voltage changes. The output voltage is well adjusted and made stiff from severe input voltage variations in both operation modes using a simple compensator. In comparison with some conventional topologies the part counts of proposed converter have been increased. However, converter reliability and small size of these components resulted from using interleave technique have compensated this detriment. Dynamic stiffness along with the capability of low-ripple I/O currents make this converter very attractive for many renewable applications like fuel cell, battery, super-capacitor, PV panel, or fuel cell energy exploitation. There is still one remaining small problem associated with the proposed converter, namely RHP zeros in the boost mode being worked to be solved and reported in the near future.

7 REFERENCES

[1] Ren, X.Y., Tang, Z., Ruan, X.B., Wei, J., Hua, G.C.: 'A novel fourswitch buck–boost converter', Proc. CSEE, 2008, 28, (21), pp. 15–19

[2] Samavatian, V; Radan, A, "A novel low-ripple interleaved buck-boost converter with high efficiency and low oscillations for fuel cell applications," Int J Electr Power Energy Syst, vol.63, pp.446, 454, Dec. 2014.

[3] R. W. Erickson and D. Maksimovic, *Fundamentals of Power Electronics*, 2nd ed. Norwell, MA: Kluwer, 2001.

[4] Carlos Restrepo, Javier Calvente, Angel Cid-Pastor, Abdelali El Aroudi, and Roberto Giral, ''A Non-Inverting Buck-Boost DC-DC Switching Converter with High Efficiency and Wide Bandwidth,''.IEEE TRANSACTIONS ON POWER ELECTRONICS, VOL. 26, NO. 9, SEPTEMBER 2011

[5] P.-C. Huang, W.-Q.Wu, H.-H.Ho, and K.-H. Chen, "Hybrid buck-boost feed forward and reduced average inductor current techniques in fast line transient and high-efficiency buck-boost converter," *IEEE Trans. Power Electron.*, vol. 25, no. 3, pp. 719–730, Mar. 2010.

[6] Y.-J. Lee, A. Khaligh, A. Chakraborty, and A. Emadi, "Digital combination of buck and boost converters to control a positive buck-boost converter and improve the output transients," *IEEE Trans. Power Electron.*, vol. 24, no. 5, pp. 1267–1279, May 2009.

[7] Y.-J. Lee, A. Khaligh, and A. Emadi, "A compensation technique for smooth transitions in a noninverting buck-boost converter," *IEEE Trans. Power Electron.*, vol. 24, no. 4, pp. 1002–1015, Apr. 2009.

[8]S. Waffler and J. Kolar, "A novel low-loss modulation strategy for high power bidirectional buck + boost converters," *IEEE Trans. Power Electron.*, vol. 24, no. 6, pp. 1589–1599, Jun. 2009.

[9] X. Ren, X. Ruan, H. Qian, M. Li, and Q. Chen, "Three-mode dual frequency two-edge modulation scheme for four-switch buck-boost converter," *IEEE Trans. Power Electron.*, vol. 24, no. 2, pp. 499–509, Feb.2009.

[10] K. I. Hwu and Y. T. Yau, "Two types of KY buck–boost converters," *IEEE Trans. Ind. Electron.*, vol. 56, no. 8, pp. 2970–2980, Aug. 2009.

[11] Hwu, K. I.; Peng, T. J., "A Novel Buck–Boost Converter Combining KY and Buck Converters," *Power Electronics, IEEE Transactions on* , vol.27, no.5, pp.2236,2241, May 2012.

[12]Blanes, J.M.; Gutierrez, R.; Garrigos, A.; Lizan, J.L.; Cuadrado, J.M., "Electric Vehicle Battery Life Extension Using Ultracapacitors and an FPGA Controlled Interleaved Buck–Boost Converter," *Power Electronics, IEEE Transactions on* , vol.28, no.12, pp.5940,5948, Dec. 2013

[13]Younghoon Cho; Jih-Sheng Lai, "High-Efficiency Multiphase DC–DC Converter for Fuel-Cell-Powered Truck Auxiliary Power Unit," *Vehicular Technology, IEEE Transactions on* , vol.62, no.6, pp.2421,2429, July 2013

[14]Liao, H.-K.; Liang, T.-J.; Yang, L.-S.; Chen, J.-F., "Non-inverting buck–boost converter with interleaved technique for fuel-cell system," *Power Electronics, IET* , vol.5, no.8, pp.1379,1388, September 2012 doi: 10.1049/iet-pel.2011.0102

[15]Mingzhi He; Fei Zhang; JianpingXu; Ping Yang; Tiesheng Yan, "High-efficiency two-switch tri-state buck-boost power factor correction converter with fast dynamic response and low-inductor current ripple," *Power Electronics, IET* , vol.6, no.8, pp.1544,1554, September 2013

[16] Ma, D., Ki, W.: 'Fast-transient PCCM switching converter with free wheel switching control', IEEE Trans. Circuits Syst. II, Express Briefs, 2007, 54, (9), pp. 825–829

[17]Viswanathan, K., Oruganti, R., Srinivasan, D.: 'Dual-mode control of tri-state boost converter for improved performance', IEEE Trans. Power Electron, 2005, 20, (4), pp. 790–797

[18]Cai-Yang Ko; Tsorng-Juu Liang; Kai-Hui Chen; Jiann-Fuh Chen, "Design and analysis of an interleave controlled series buck converter with low load current ripple," *Circuits and Systems (APCCAS), 2010 IEEE Asia Pacific Conference on* , vol., no., pp.672,675, 6-9 Dec. 2010

[19] Xiao, H.; Xie, S., "Interleaving double-switch buck-boost converter," *Power Electronics, IET*, vol.5, no.6, pp.899,908, July 2012

[20] Po-Wa Lee; Lee, Y. -S; Cheng, D.K.-W.; Xiu-Cheng Liu, "Steady-state analysis of an interleaved boost converter with coupled inductors," *Industrial Electronics, IEEE Transactions on* , vol.47, no.4, pp.787,795, Aug 2000

[21] Hajizadeh, A.; Golkar, M.A.; Feliachi, A., "Voltage Control and Active Power Management of Hybrid Fuel-Cell/Energy-Storage Power Conversion System Under Unbalanced Voltage Sag Conditions," *Energy Conversion, IEEE Transactions on* , vol.25, no.4, pp.1195,1208, Dec. 2010

[22] Miwa, Brett A.; Otten, D.M.; Schlecht, M.F., "High efficiency power factor correction using interleaving techniques," *Applied Power Electronics Conference and Exposition, 1992. APEC '92. Conference Proceedings 1992., Seventh Annual*,vol., no., pp.557, 568, 23-27 Feb 1992

[23]J. Calvente, L. Martinez-Salamero, P. Garces, and A. Romero, "Zero dynamics-based design of damping networks for switching converters," *IEEE Trans. Aerosp. Electron. Syst.*, vol. 39, no. 4, pp. 1292–1303, Oct. 2003.

[24]Veerachary, M., "General rules for signal flow graph modeling and analysis of dc-dc converters," *Aerospace and Electronic Systems, IEEE Transactions on* , vol.40, no.1, pp.259,271, Jan 2004

[25] Veerachary, M., "Modeling of Power Electronic Systems Using Signal Flow Graphs," *IEEE Industrial Electronics, IECON 2006 - 32nd Annual Conference on* , vol., no., pp.5307,5312, 6-10 Nov. 2006

[26] Veerachary, M.; Senjyu, T.; Uezato, K., "Signal flow graph modelling of DC-DC parallel converter with coupled inductors," *Power Conversion Conference, 2002. PCC-Osaka 2002. Proceedings of the*, vol.3, no., pp.1352, 1356 vol.3, 2002

[27] Veerachary, M., "Analysis of interleaved dual boost converter with integrated magnetics: signal flow graph approach," *Electric Power Applications, IEE Proceedings - *, vol.150, no.4, pp.407,416, 8 July 2003

[28] Veerachary, M.; Senjyu, T.; Uezato, K., "Signal flow graph nonlinear modelling of interleaved converters," *Electric Power Applications, IEE Proceedings - *, vol.148, no.5, pp.410, 418, Sep 2001

[29] Veerachary, M.; Senjyu, T.; Uezato, K., "Signal flow graph nonlinear modeling analysis of IDB converter [interleaved dual boost]," *Industrial Electronics, 2001. Proceedings.ISIE 2001. IEEE International Symposium on*, vol.2, no., pp.1066, 1070 vol.2, 2001